Predistortion for Very Low Pulse-Compression Sidelobes in Solid-State Meteorological Radar

Predistortion for Very Low Pulse-Compression Sidelobes in Solid-State Meteorological Radar

Stephen J. Frasier, *Senior Member, IEEE*, Fabrizio Argenti, *Senior Member, IEEE*, and Luca Facheris

***Abstract*— In this letter, we address the problem of combating the effect of the nonlinearities of the transmit–receive chain in solid-state radars, which are typically generated by the power amplifier (PA) in transmission. This issue is of particular importance in meteorological radar applications, as they require to transmit pulse featuring very low autocorrelation sidelobes, which are significantly raised due to nonlinearities. In this work, we describe an adaptive predistortion design method based on an iterative approach in the spectral domain. The proposed method has been validated by means of hardware using a customized software radio and driving an amplifier into saturation. Two different ideal, highly performing pulse compression waveforms, expressly designed for weather radar applications, were sent to its input. The experimental results demonstrate the benefits of the proposed approach to design the digital predistortion module.**

***Index Terms*— Digital predistortion, pulse compression, solid-state power amplifier (PA), weather radar.**

I. Introduction

PULSE compression is a key aspect of solid-state meteorological radar systems. Through pulse compression, it is possible to reduce the transmit peak power with respect to a much shorter unmodulated pulse while keeping a constant transmit energy. Therefore, resorting to pulse compression becomes mandatory in order to jointly maintain the desired range resolution and level of sensitivity. A remarkable issue related to the design of pulse compression waveforms for the aforementioned systems is achieving the requisite range sidelobe levels. As a matter of fact, the dynamic range of the weather echo is very large and can be highly variable in range, with strong gradients [1], [2], hence the need to reduce range sidelobes to levels typically below −60 dB or more.

The topic of low-sidelobe waveforms has been dealt with by several authors (e.g., [2], [3], [4]). To achieve the objective, a phase or frequency modulation is introduced in a constant amplitude transmit pulse. In this way, the autocorrelation function (ACF) obtained at the output of a matched filter receiver changes from a triangular shape to one featuring a central narrow mainlobe and lower sidelobes. Recently, an iterative design method able to provide waveforms whose ACFs exhibit particularly low sidelobes has been presented in [5]. Amplitude tapering (windowing) or, in general, a mismatched receive filter can also be introduced in order to further reduce the level of the sidelobes, at the expense of some peak level reduction and broadening of the mainlobe [6].

Unfortunately, whatever the ideal waveform, in practical implementations the sidelobes level may increase significantly due to a nonlinear behavior of the transmit–receive chain [7]; in practice, the major contribution to distortion is produced by the power amplifier (PA) of the transmitter. To ensure that the signal exciting the transmitter provides the desired ACF properties at the receiver output, some sort of controlled distortion must be applied to the transmit waveform through a digital predistortion device (DPD). The typical DPD design approach requires the modeling of the nonlinear characteristics of the transmit–receive chain, which may include memory effects. Various models are available to characterize nonlinear effects, including the Volterra, Hammerstein, Wiener, and Memory Polynomial models [8], [9], [10], [11]. In this work, we utilize an alternative adaptive predistortion method, based on a spectral correction factor applied iteratively to the original ideal waveform. The solution is particularly simple and provides remarkable results.

This letter is organized as follows. In Section II the adaptive DPD construction is presented; in Section III, the hardware used to realize the transmit/receive chain is described; Section IV shows the results of the DPD implementation, which is further discussed in Section V. Concluding remarks are drawn in Section VI.

II. Adaptive Predistortion Implementation

The synthesis of the predistorted waveform is done in the frequency domain. The block diagram describing the proposed method is depicted in Fig. 1, where: PA denotes the power amplifier and G denotes the PA gain; $X(f)$ represents the Fourier transform of the ideal signal $x(t)$, i.e., the output of the pulse compression waveform design process; the DPD block is a device that generates the predistorted waveform (hereafter, DPD waveform). For the sake of simplicity, in the following, we will assume that $G = 1$ (or, in other words, that the gain of the amplifier is removed by normalizing all waveforms).

The output of a distortionless PA would be identical to $x(t)$, but scaled by the gain of the amplifier. Let $Y_0(f)$ be the Fourier transform of the PA output when the input is $x(t)$. If the PA

Manuscript received 26 January 2023; revised 23 March 2023; accepted 28 March 2023. Date of publication 31 March 2023; date of current version 12 April 2023. *(Corresponding author: Luca Facheris.)*

Stephen J. Frasier is with the Department of Electrical and Computer Engineering, University of Massachusetts Amherst, Amherst, MA 01003 USA (e-mail: frasier@umass.edu).

Fabrizio Argenti and Luca Facheris are with the Department of Information Engineering, University of Florence, 50139 Florence, Italy (e-mail: fabrizio.argenti@unifi.it; luca.facheris@unifi.it).

Digital Object Identifier 10.1109/LGRS.2023.3263678

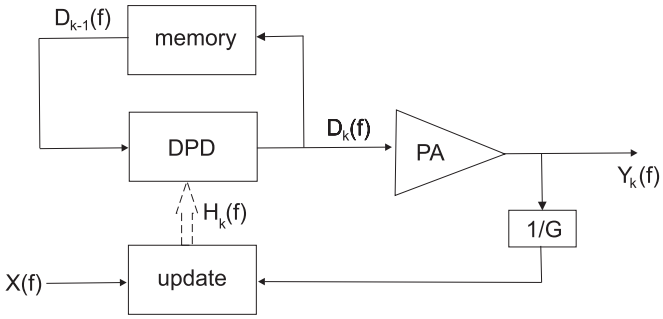

Fig. 1. Block diagram of adaptive DPD implementation.

introduced only linear distortion, then the DPD design problem would be solved by a simple inverse filter. In other terms, the DPD transfer function would be

$$H_0(f) = \frac{X(f)}{Y_0(f)}. \tag{1}$$

The proposed iterative procedure attempts to design a DPD such that the cascade of DPD and PA works as an identity system for the given ideal $X(f)$.

Let $H_k(f)$ be the DPD transfer function at iteration k and let $D_k(f)$ be the DPD waveform at the same iteration. The iterative procedure is initialized by using (1), so that the Fourier transform of the first DPD waveform is given by

$$D_1(f) = X(f)H_0(f). \tag{2}$$

Running this waveform through the amplifier produces $y_1(t)$ with Fourier transform $Y_1(f)$. At the kth iteration, the DPD frequency response is updated as follows:

$$H_k(f) = \frac{X(f)}{Y_k(f)} \tag{3}$$

and copied into the DPD block. Therefore, the Fourier transform of the DPD waveform changes as follows:

$$D_{k+1}(f) = H_k(f)D_k(f). \tag{4}$$

Such equation includes also (2) by assuming $D_0(f) = X(f)$. After N iterations, the DPD waveform's Fourier transform is given by

$$D_N(f) = X(f)\prod_{k=0}^{N-1} H_k(f) = X(f)\bar{H}_N(f) \tag{5}$$

where, by using (3), we have

$$\bar{H}_N(f) = \prod_{k=0}^{N-1} H_k(f) = \prod_{k=0}^{N-1} \frac{X(f)}{Y_k(f)}. \tag{6}$$

From these equations, the following observations, which justify the proposed method, can be made. Assume that convergence of the iterative equations is reached and let $D_\infty(f)$ be the final DPD waveform. Such a function, which does not significantly change as k increases, is the objective of our search, since it is the predistorted waveform that produces $X(f)$ at the output of the PA. In fact, according to (4), when convergence is reached, $H_k(f)$ tends to $H_\infty(f) = 1$ and, from (3), we have that the output of the PA is given by

$$Y_\infty(f) = X(f) \tag{7}$$

which is the ideal waveform we would actually like to transmit, even in the presence of a distorting device. From (5), we also observe that $D_\infty(f)$ is obtained by filtering $X(f)$ with $\bar{H}_\infty(f)$.

As the procedure operates on the complex spectrum of the input waveform, it modifies both its amplitude and phase. The validity of the proposed method has been assessed by using a real amplifier driven into saturation as described in Sections III and IV.

III. Hardware Description

The hardware used for testing the proposed method is the Universal Software Radio Peripheral (USRP) model N210 by Ettus Research [12]. The University of Massachusetts has employed and customized this for use as an intermediate-frequency digital transceiver in a number of radar systems. The unit consists of a main board that includes a Xilinx[1] Spartan[1] 3A-DSP 3400 field programmable gate array (FPGA), 100 MS/s dual analog-to-digital converters (ADCs), 400 MS/s dual digital to analog converters (DACs), and gigabit ethernet connectivity to stream data to and from a host computer.

The FPGA hosts a digital upconverter (DUC) and digital downconverter (DDC), an RF front-end that interfaces to ADCs and DACs, and a baseband packet engine that interfaces to ethernet. All components are open source, which permits ease of customization. Our customizations included the ability to upload an arbitrary baseband complex waveform at a prescribed sampling frequency. This waveform is upconverted to a desired center frequency and is transmitted upon receipt of a trigger. Center frequencies and sampling bandwidths for the ADC and DAC are programmable. Also with each trigger, a prescribed number of baseband samples are captured, timestamped, and uploaded to the host computer.

Fig. 2 shows the photograph of the hardware setup. The waveform transmitted by the DAC is input to an RF amplifier which is driven into saturation. At the output of the amplifier, a 20-dB attenuator is followed by a low-pass filter with 50 MHz cutoff to suppress harmonics that might alias back into the band of interest. The attenuation was included to isolate the amplifier from the filter. Reflected energy from the filter input is suppressed by an additional 20 dB. While this testbed is rather simple and lacks several components that would exist in a real radar system (e.g., up and downconverters between intermediate and radio frequencies, receiver chain), the primary source of the nonlinearity is the PA which is usually driven into saturation. All other components in a radar system are designed to operate in their linear regions. Thus, this setup captures the essential nonlinear behavior.

For the experiments here, the waveform was transmitted and received at a center frequency of 40 MHz with baseband samples specified at a sampling rate of 12.5 MS/s. In the DDC, this corresponds to filtering and decimation by a factor of

[1]Registered trademark.

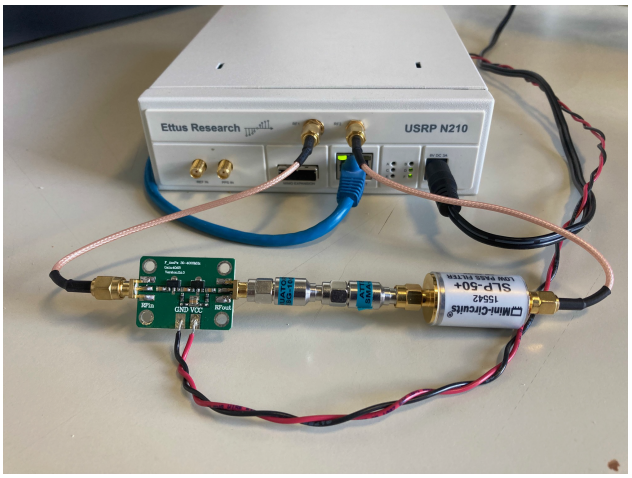

Fig. 2. Photograph of the experimental setup. The baseband waveform is sent to the N210 via ethernet and is digitally upconverted to a 40 MHz center frequency. The signal path is then from the N210 DUC output through the amplifier, attenuators, and lowpass filter to the N210 DDC input. Received data are sampled at 100 MHz, digitally filtered, downconverted to baseband, and recorded to the host computer via ethernet.

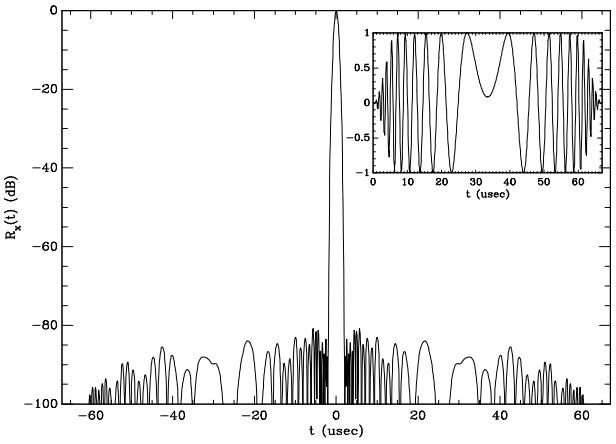

Fig. 3. *Example 1:* Autocorrelation of NLFM waveform whose in-phase component is shown in the inset.

8 from the 100 MS/s rate of the ADCs. In order to improve the signal-to-noise ratio in the receiver, 100 pulses were coherently integrated on the host computer to make up for the 20 dB of attenuation between the amplifier and the filter.

Two nonlinear frequency-modulated (NLFM) pulse waveforms were considered to assess the performance of the proposed method. They differ for both duration and swept bandwidth, but exhibit narrow mainlobe and sidelobe levels around −80 dB. The two waveforms were designed following the method described in [5] and their parameters are shown in Table I.

Example 1: The duration is 67 μs and the swept bandwidth is 2.2 MHz. This waveform and its autocorrelation are shown in Fig. 3.

Example 2: The duration is 40 μs and the swept bandwidth is 5 MHz. This waveform and its autocorrelation are shown in Fig. 4.

The nonlinear effect of the amplifier is evidenced in Fig. 5, with reference to the waveform of Example 1. Fig. 5(a) shows

TABLE I
WAVEFORM PARAMETERS

	Example 1	Example 2
Swept Bandwidth (MHz)	2.2	5
Duration (μs)	67	40
Tukey rolloff factor	0.2	0.15
Null-to-null ACF mainlobe width (μs)	4.1	1.8
Baseband Sampling Frequency (MS/s)	12.5	12.5

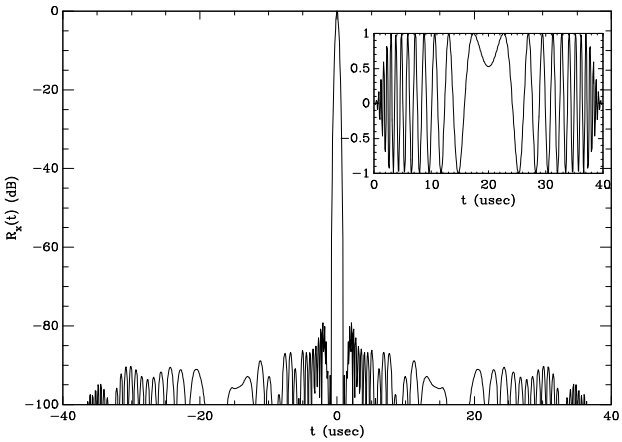

Fig. 4. *Example 2:* Autocorrelation of NLFM waveform whose in-phase component is shown in the inset.

the envelopes of the input and output waveforms without predistortion. The plot is scaled such that the small-signal gain of the overall system is unity. The amplifier saturates at a level that is 4.2 dB compressed from unity gain. This is shown another way in Fig. 5(b), which shows the output power versus input power. The rising edge of the waveform traces along the unity gain line (dashed) until it saturates, then droops during the constant amplitude portion of the input waveform. The falling edge of the waveform traces slightly below the unity gain line by an amount approximately equal to the droop.

IV. RESULTS

In this section, we present the results obtained with the proposed adaptive technique for DPD design. With reference to the waveform of Example 1, Fig. 6 shows the ACF of the output waveform from the PA for the zeroth, fifth, and tenth iteration of the learning. The initial iteration shows the degradation of sidelobes due to the distortion of the PA, with peak sidelobes just below −45 dB (black line). The effect of the iterative predistortion approach is that initially, the highest sidelobes nearest the main lobe are suppressed at the expense of some increase of sidelobes further away from the main lobe (red line). After additional iterations, all of the sidelobes (blue line) are reduced nearly to the design level (black dashed line).

For better understanding of the iterative process, in Fig. 7, we show, still with reference to Example 1, the final predistorted input envelope along with the resulting output envelope, which now mimics the shape of the original input, but at the saturated output level. The predistorter serves to reduce the (linear) gain of the amplifier by an amount equal to the gain compression of the output. While the gain is significantly

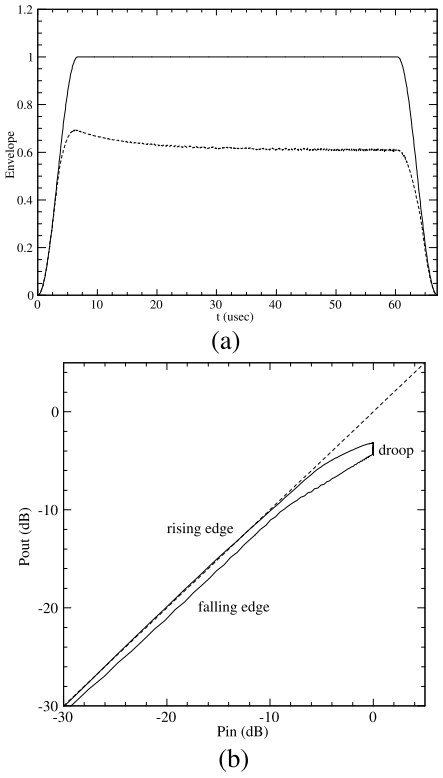

Fig. 5. *Example 1:* (a) Envelope of the input waveform (solid line) and of the output waveform (dashed) without predistortion (following the initial droop, the output amplitude is compressed 4.2 dB). (b) Input–output power characteristic of the PA without predistortion; note the relationship is multivalued due to the droop.

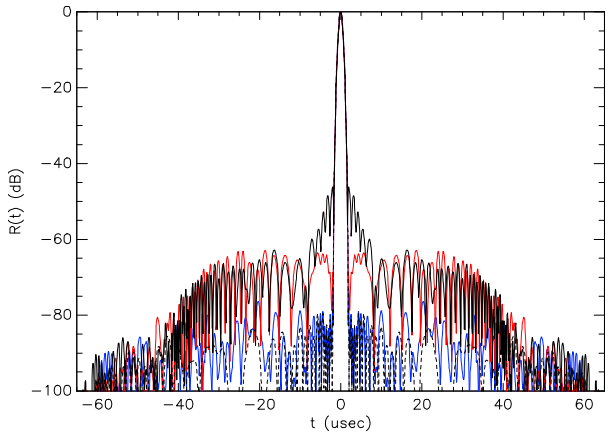

Fig. 6. Autocorrelation of the output waveform for *Example 1:* (Black) Initial iteration, (red) fifth iteration, (blue) tenth iteration, and (black dashed) ideal waveform.

reduced, it should be noted that this affects only the rising and falling edges of the waveform. Most of the waveform's duration is still spent at the saturated output level. The resulting energy loss is small, in this case 0.3 dB, and is due to the lack of overshoot evident in the original output.

The DPD design procedure applied to the waveform of Example 2 yields a similar learning evolution, as demonstrated in Fig. 8. In this case, the input drive level is 3 dB higher than in Example 1, and we find that approximately twice as many iterations are necessary to achieve the desired sidelobe levels.

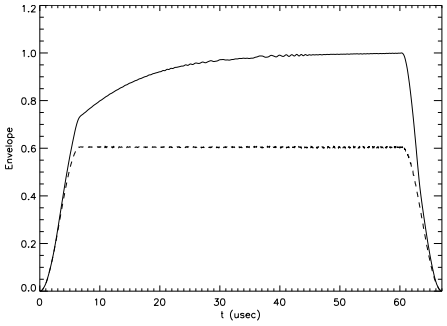

Fig. 7. *Example 1:* (Solid line) Envelope of the predistorted input waveform and (dashed) resulting output waveform.

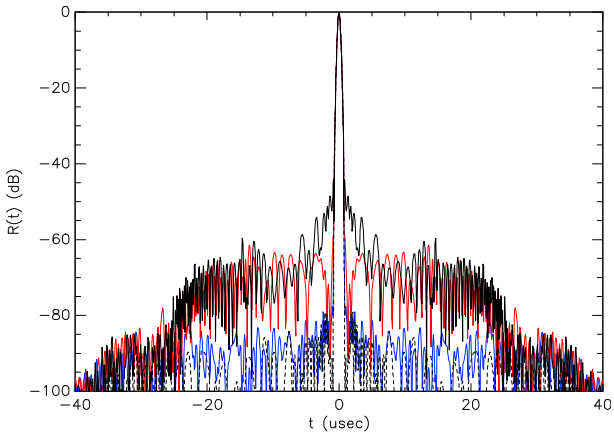

Fig. 8. Autocorrelation of the output waveform for *Example 2:* (Black) Initial iteration, (red) 11th iteration, (blue) 23rd iteration, and (black dashed) ideal waveform.

Figs. 9 and 10 are analogous to Figs. 5 and 7 for Example 2. In this case, the output is further compressed by 6.5 dB and the energy loss is about 0.7 dB. In both cases, the droop of the output waveform is evidence that the amplifier is in saturation.

V. Implementation Considerations

Implementing the proposed technique on a real solid-state radar system requires characterizing enough of the transmitter and receiver to capture the nonlinearities. A complete characterization of the entire system would require an external target, such as a corner reflector, placed at a range just beyond the blind range of the pulse compression waveform. This target, likely several kilometers distant from the radar, would need to present a signal-to-noise ratio and a signal-to-clutter ratio sufficient to observe the desired sidelobes, which is not straightforward. It is not necessary to capture the entire transmit/receive chain, however. Components that may be reliably assumed to be distortionless may be omitted. For example, we found that operating our testbed with the amplifier in its linear range had a negligible effect on sidelobes without any predistortion.

The radar may include an internal calibration loop that samples the output of the PA and attenuates it to a level acceptable to the receiver front-end. This is fairly straightforward on a conventional radar employing a reflector antenna. The loop

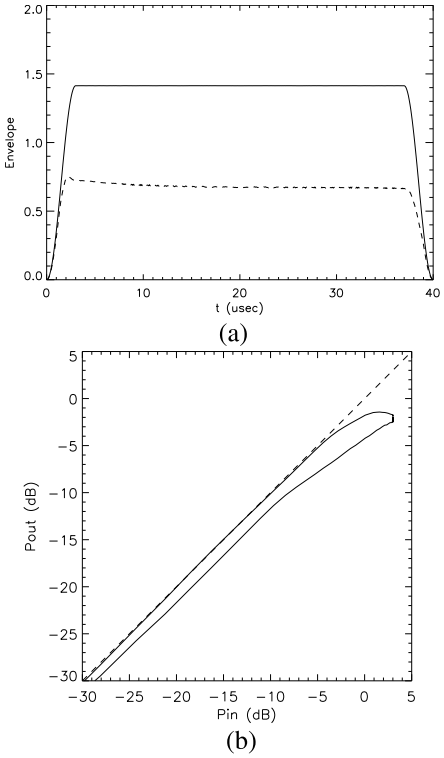

Fig. 9. *Example 2:* (a) Without predistortion as in Fig. 6(a). Input drive level is twice the previous case. After the initial droop, the output is compressed by 6.5 dB. (b) As in Fig. 6(b).

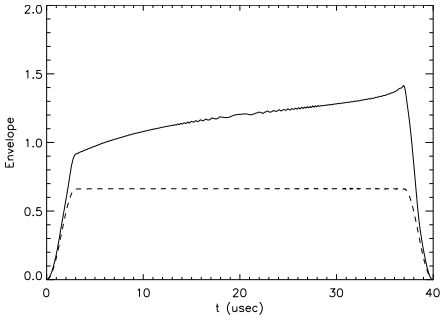

Fig. 10. *Example 2:* With predistortion as in Fig. 7.

would consist of a directional coupler at the PA output, attenuator, and a switch preceding the receiver to select between the calibration loop and the receiving antenna. This loop would necessarily exclude the antenna and transmit/receive switch. It could even exclude the receiver low-noise amplifier which is likely very linear.

The situation is considerably more complicated on an active phased-array radar where there are many PAs whose outputs are combined in a direction-dependent fashion and where there are both series and parallel sources of nonlinearity [13], [14]. Treatment of this case is beyond the scope of this letter.

VI. Conclusion

In this letter, we have investigated the nonlinear effects of a saturated amplifier on NLFM waveforms designed for meteorological radar systems exhibiting highly desirable pulse compression features. An iterative method for designing a digital predistorter that creates a waveform able to compensate for the nonlinear effects has been proposed. The method has been tested and validated on a hardware testbed working at intermediate frequency using two different pulse waveforms designed by the authors in another study, and at two different drive levels beyond the 1 dB compression point of the amplifier. The method converges with a reasonable number of iterations to a final solution with pulse compression characteristics very close to the ideal ones. We find that the rate of convergence is correlated with the amount of nonlinearity which is reasonably expected.

References

[1] V. N. Bringi and V. Chandrasekhar, *Polarimetric Doppler Weather Radar: Principles and Applications*. Cambridge, U.K.: Cambridge Univ. Press, 2001.

[2] J. M. Kurdzo, B. L. Cheong, R. D. Palmer, G. Zhang, and J. B. Meier, "A pulse compression waveform for improved-sensitivity weather radar observations," *J. Atmos. Ocean. Technol.*, vol. 31, no. 12, pp. 2713–2731, Dec. 2014.

[3] C. Pang et al., "A pulse compression waveform for weather radars with solid-state transmitters," *IEEE Geosci. Remote Sens. Lett.*, vol. 12, no. 10, pp. 2026–2030, Oct. 2015.

[4] S. M. Torres, C. D. Curtis, and D. Schvartzman, "Requirement-driven design of pulse compression waveforms for weather radars," *J. Atmos. Ocean. Technol.*, vol. 34, no. 6, pp. 1351–1369, Jun. 2017.

[5] F. Argenti and L. Facheris, "Radar pulse compression methods based on nonlinear and quadratic optimization," *IEEE Trans. Geosci. Remote Sens.*, vol. 59, no. 5, pp. 3904–3916, May 2021.

[6] C. E. Cook and M. Bernfeld, *Radar Signals: An Introduction to Theory and Application*. Norwood, MA, USA: Artech House, 1993.

[7] D. Schvartzman and S. Torres, "Design of practical pulse compression waveforms for polarimetric phased array radar," in *Proc. 39th Int. Conf. Radar Meteorol.*, Nara, Japan, 2019, pp. 1–19, Paper 15A-02.

[8] D. R. Morgan, Z. Ma, J. Kim, M. G. Zierdt, and J. Pastalan, "A generalized memory polynomial model for digital predistortion of RF power amplifiers," *IEEE Trans. Signal Process.*, vol. 54, no. 10, pp. 3852–3860, Oct. 2006.

[9] L. Ding et al., "A robust digital baseband predistorter constructed using memory polynomials," *IEEE Trans. Commun.*, vol. 52, no. 1, pp. 159–165, Jan. 2004.

[10] A. Zhu and T. J. Brazil, "An overview of Volterra series based behavioral modeling of RF/microwave power amplifiers," in *Proc. IEEE Annu. Wireless Microw. Technol. Conf.*, Dec. 2006, pp. 1–5.

[11] F. M. Ghannouchi, O. Hammi, and M. Helaoui, *Behavioral Modeling and Predistortion of Wideband Wireless Transmitters*. Hoboken, NJ, USA: Wiley, 2015.

[12] *USRP N210 Software Defined Radio*. [Online]. Available: https://www.ettus.com/all-products/un210-kit/

[13] N. Tervo et al., "Digital predistortion concepts for linearization of mmW phased array transmitters," in *Proc. 16th Int. Symp. Wireless Commun. Syst. (ISWCS)*, Aug. 2019, pp. 325–329.

[14] N. Tervo et al., "Digital predistortion of phased-array transmitter with shared feedback and far-field calibration," *IEEE Trans. Microw. Theory Techn.*, vol. 69, no. 1, pp. 1000–1015, Jan. 2021.

Open Access funding provided by 'Università degli Studi di Firenze' within the CRUI CARE Agreement